© 2022. Published by The Company of Biologists Ltd | Journal of Experimental Biology (2022) 225, jeb243216. doi:10.1242/jeb.243216

RESEARCH ARTICLE

2D and 3D visualizations of archosaur jaw muscle mechanics, ontogeny and phylogeny using ternary diagrams and 3D modeling

Ian N. Cost[1,2,*,‡], Kaleb C. Sellers[1,3,*,‡], Rachel E. Rozin[1,4], Anthony T. Spates[1,5], Kevin M. Middleton[1] and Casey M. Holliday[1]

ABSTRACT

Comparing patterns of performance and kinematics across behavior, development and phylogeny is crucial to understand the evolution of complex musculoskeletal systems such as the feeding apparatus. However, conveying 3D spatial data of muscle orientation throughout a feeding cycle, ontogenetic pathway or phylogenetic lineage is essential to understanding the function and evolution of the skull in vertebrates. Here, we detail the use of ternary plots for displaying and comparing the 3D orientation of muscle data. First, we illustrate changes in 3D jaw muscle resultants during jaw closing taxa the American alligator (*Alligator mississippiensis*). Second, we show changes in 3D muscle resultants of jaw muscles across an ontogenetic series of alligators. Third, we compare 3D resultants of jaw muscles of avian-line dinosaurs, including extant (*Struthio camelus*, *Gallus gallus*, *Psittacus erithacus*) and extinct (*Tyrannosaurus rex*) species to outline the reorganization of jaw muscles that occurred along the line to modern birds. Finally, we compare 3D resultants of jaw muscles of the hard-biting species in our sample (*A. mississippiensis*, *T. rex*, *P. erithacus*) to illustrate how disparate jaw muscle resultants are employed in convergent behaviors in archosaurs. Our findings show that these visualizations of 3D components of jaw muscles are immensely helpful towards identifying patterns of cranial performance, growth and diversity. These tools will prove useful for testing other hypotheses in functional morphology, comparative biomechanics, ecomorphology and organismal evolution.

KEY WORDS: Archosaur, Ternary diagram, Biomechanics, 3D visualization, Orientation

INTRODUCTION

Recent advances in imaging and computational methods are enabling researchers to capture three-dimensional (3D) morphology at high resolutions. Researchers are ushering in a renaissance of imaging approaches in areas such as astronomy (Cohen et al., 2003; Preusker et al., 2015; Korsun et al., 2016), biochemistry (Lüthy et al., 1992; Zemla, 2003; Arnold et al., 2006), and archaeology and anthropology (Hughes et al., 2005; Lee et al., 2007; Carlson et al., 2011; Du Plessis et al., 2015). Similarly, biological sciences are greatly enhanced by morphological studies incorporating large amounts of high-resolution 3D data. Morphologists frequently model diverse morphological systems in entomology (Klaus et al., 2003; Friedrich and Beutel, 2008), physiology (Witmer et al., 1999; Schachner et al., 2013; Tsai and Holliday, 2015; Stephenson et al., 2017), neuroanatomy (Evans et al., 2009; Lautenschlager et al., 2012; Kawabe et al., 2013) and skeletal tissue biomechanics (Grosse et al., 2007; Cuff et al., 2015) using high-resolution data. Modeling musculoskeletal systems in 3D is now enabling researchers to investigate the underlying biomechanics of behaviors, such as feeding (Gans et al., 1985; Zusi, 1987; Witmer and Rose, 1991; Hoese and Westneat, 1996; Herrel et al., 1999; Dumont et al., 2005; Dawson et al., 2011; Snively et al., 2013; Sellers et al., 2017; Bates and Falkingham, 2018; Cost et al., 2020) and locomotion (Hutchinson, 2004; Charles et al., 2016; Manafzadeh and Padian, 2018), using computational and imaging methods such as finite element analysis (e.g. Keyak et al., 1993; Rayfield, 2007; Santana et al., 2010), XROMM (e.g. Brainerd et al., 2010; Baier et al., 2013) and multibody dynamics (e.g. Moazen et al., 2009; Curtis et al., 2010; Snively et al., 2015).

Shared among many biomechanical studies is the measurement and visualization of the magnitudes (e.g. Newtons) and orientations of forces (e.g. x, y, z), often across time (t). Biologists often report the most biomechanically and ecologically important portions of forces, such as the vertical (orthal) component of bite force or vertical component of ground-reaction force. Additionally, we also often disregard component forces in the transverse or axial planes, in part as a product of the historical focus on mammalian feeding and locomotor systems where muscles largely act in parasagittal planes (e.g. Maynard Smith and Savage, 1959; Dullemeijer, 1956; Cartmill, 1974, 1985) relative to the systems in other vertebrates. But also, pragmatically, it is simply challenging to visualize all force components simultaneously or in a fashion understandable by readers in traditional publishing. Thus, the complicated 3D nature of musculoskeletal anatomy remains difficult to convey in two-dimensional (2D) publications and other media (e.g. Greaves, 1982; Sinclair and Alexander, 1987; Bimber et al., 2002; Lockwood et al., 2002; Holliday and Witmer, 2007; Vincent et al., 2007; Huber et al., 2008; Sustaita, 2008; Holliday, 2009; Kolmann and Huber, 2009; Pfaller et al., 2011; Figueirido et al., 2013; Holliday et al., 2013; Cost et al., 2020). The solution has been to decompose multidimensional measurements into more simplified plots that are designed specifically for 2D publishing including iterative columns, box plots and line graphs. This, in turn, causes higher-order questions of behavior, ontogeny and phylogeny to be even more challenging to analyze and disseminate. One solution is to project 3D force components in a ternary diagram. Ternary diagrams have a long history of

[1]Department of Pathology and Anatomical Sciences, University of Missouri, Columbia, MO 65211, USA. [2]Department of Biology, Albright College, Reading, PA 19612, USA. [3]Department of Clinical Anatomy and OPP, Rocky Vista University, Parker, CO 80134, USA. [4]Florida Aquarium, Tampa, FL 33602, USA. [5]University of Missouri Kansas City School of Dentistry, Kansas City, MO 64108, USA.
*These authors contributed equally to this work

‡Authors for correspondence (icost@albright.edu; ksellers@rvu.edu)

I.N.C., 0000-0002-5087-6823; K.C.S., 0000-0002-3588-9562; K.M.M., 0000-0003-4704-1064; C.M.H., 0000-0001-8210-8434

Received 28 July 2021; Accepted 20 December 2021

Journal of Experimental Biology (2022) 225, jeb243216. doi:10.1242/jeb.243216

List of symbols and abbreviations

3D	three-dimensional
2D	two-dimensional
CT	computed tomography
mAMEM	m. adductor mandibulae externus medialis
mAMEP	m. adductor mandibulae externus profundus
mAMES	m. adductor mandibulae externus superficialis
mAMP	m. adductor mandibulae posterior
mDM	m. depressor mandibulae
mEM	m. ethmomandibularis
mPTd	m. pterygoideus dorsalis
mPSTs	m. pseudotemporalis superficialis
mPSTp	m. pseudotemporalis profundus
PCSA	physiological cross-sectional area
STL	stereolithographic
XROMM	x-ray reconstruction of moving morphology
x_{ins}	*x* insertion
x_{or}	*x* origin
y_{ins}	*y* insertion
y_{or}	*y* origin
z_{ins}	*z* insertion
z_{or}	*z* origin
µCT	microcomputed tomography

use in geology, chemistry and physics, wherein the relative contributions of three variables to a whole are studied. For example, phases of matter (Othmer and Tobias, 1942), soil composition (Norton, 1966), vertebrate limb proportions (Gatesy and Middleton, 1997, 2008; Middleton and Gatesy, 2000) and ventilation kinematics (Capano et al., 2019) have made use of ternary diagrams in the past.

Here, we use ternary diagrams to provide examples of how jaw muscle resultants (a summation vector composed of the contributing forces applied to a muscle across multiple planes and directions) of archosaurs (crocodylians, dinosaurs, and birds) change over time using three case studies of behavior, ontogeny and phylogeny. First, within a single individual, the 3D nature of the cranial musculature requires that muscle forces and resultants must vary with gape (Herring and Herring, 1974; Dumont and Herrel, 2003) during a feeding bout. We demonstrate how ternary plots enable researchers to visualize the changes in orientations through one open-to-close phase of a feeding cycle in *Alligator mississippiensis*. Second, archosaurs have a wide diversity of cranial morphologies and feeding ecologies that change during ontogeny (see Fig. 1; Erickson et al., 2003; Yanega and Rubega, 2004; Grigg and Kirshner, 2015). Here, we show that ternary plots are able to track the trajectory of muscle orientation change through ontogeny in alligators. Third, comparisons across geological time reveal broad patterns among Archosauria including repeated evolution of large body size (Turner and Nesbitt, 2013), convergent evolution of feeding ecologies (Burton, 1974) and relatively hard biting in diverse clades (e.g. Carril et al., 2015; Sellers et al., 2017; Bates and Falkingham, 2018, Cost et al., 2020). We plotted the orientations of jaw muscles across a sample of living and extinct dinosaurs to illustrate their morphological disparity and, as a proof of concept, to demonstrate how ternary diagrams can be used to compare related taxa across time. Finally, we also compare the jaw muscle resultants of hard-biting species to demonstrate how convergence in behavior can occur using very different jaw muscle configurations. We show that ternary diagrams are particularly useful for conveying components of jaw muscle resultants at different scales of organization, enabling comparisons of higher-order biomechanical data across behavior, ontogeny and phylogeny. More broadly, ternary diagrams can represent complex 3D structures or forces in a 2D space such that anatomical relationships and physiological parameters are retained as comparable data.

MATERIALS AND METHODS

Specimens and imaging

The skulls of four extant taxa (American alligator, *Alligator mississippiensis*: MUVCAL008, MUVCAL024, MUVCAL031, MUVCAL612, MUVCAL622, MUVCAL700; Common ostrich, *Struthio camelus*: OUVC10659; Domestic chicken, *Gallus gallus*: MUVCAV003; and Grey parrot, *Psittacus erithacus*: MUVCAV042, MUVCAV092) and one extinct taxon (*Tyrannosaurus rex*: BHI3033) were scanned using computed tomography (CT) or micro-computed tomography (µCT; Table 1). Specimens of alligator (MUVCAL031), chicken (MUVCAV003) and parrot (MUVCAV042) were µCT scanned at the Truman VA Biomolecular Imaging Center, in Columbia, MO (Siemens Inveon MicroCT, Siemens Medical Solutions USA Inc., Malvern, PA, USA). The largest alligator specimen (MUVCAL008) was CT scanned at the University of Missouri School of Medicine Department of Radiology (Siemens Somatom Definition Scanner, Siemens Medical Solutions USA Inc., Malvern, PA, USA). All other alligator specimens (MUVCAL024, MUVCAL612, MUVCAL622, MUVCAL700) were CT scanned at the University of Missouri School of Veterinary Medicine (GE LightSpeed VCT CT scanner, GE Medical, Milwaukee, WI, USA; Sellers et al., 2017). A second parrot specimen (MUVCAV092) was µCT scanned at the University of Missouri Department of Geological Sciences X-ray Microanalysis Core (Zeiss Xradia 510 Versa 3D x-ray microscope, Carl Zeiss Microscopy, LLC, Pleasanton, CA, USA). A 1/6-scale model of *T. rex* (BHI 3033) was scanned at OhioHealth O'Bleness Memorial Hospital, Athens, OH (General Electric LightSpeed Ultra Multislice CT scanner, Milwaukee, WI, USA; Cost et al., 2020).

Jaw muscles of interest (m. adductor mandibulae externus medialis, mAMEM; m. adductor mandibulae externus profundus, mAMEP; m. adductor mandibulae externus superficialis, mAMES; m. adductor mandibulae posterior, mAMP; m. pterygoideus dorsalis, mPTd; m. pseudotemporalis superficialis, mPSTs; m. pseudotemporalis profundus, mPSTp; m. ethmomandibularis, mEM; m. depressor mandibulae, mDM) were identified through physical dissection and processed diffusible iodine contrast-enhanced CT (DiceCT; Fig. 2; Holliday et al., 2013; Gignac and Erickson, 2016). Scans were rendered and segmented using Avizo v9.5 (Thermo Fisher Scientific, Waltham, MA, USA; Fig. 3A). Defects were repaired, segmenting artifacts were removed, and a constant universal axis was applied to all models in Geomagic Studio 2013 (3D Systems, Rock Hills, SC, USA). Axes were oriented such that the *x*-axis corresponded to the mediolateral axis, the *y*-axis to the dorsoventral axis and the *z*-axis to the rostrocaudal axis. Models were then imported into Strand7 (Strand7 Pty Ltd, Sydney, NSW, AUS) where muscle attachment areas were identified and mapped on 3D finite element model (Fig. 3B and Fig. 4). Finite element analysis (FEA) software was used for muscle mapping to facilitate incorporation of muscle reconstruction data into subsequent analyses following the methods of Grosse et al. (2007) and Davis et al. (2010). Muscle maps (Fig. 4) were estimated from direct observations of material (dissections, DiceCT; see Fig. 2), interpretations of osteological correlates and the literature,

Journal of Experimental Biology (2022) 225, jeb243216. doi:10.1242/jeb.243216

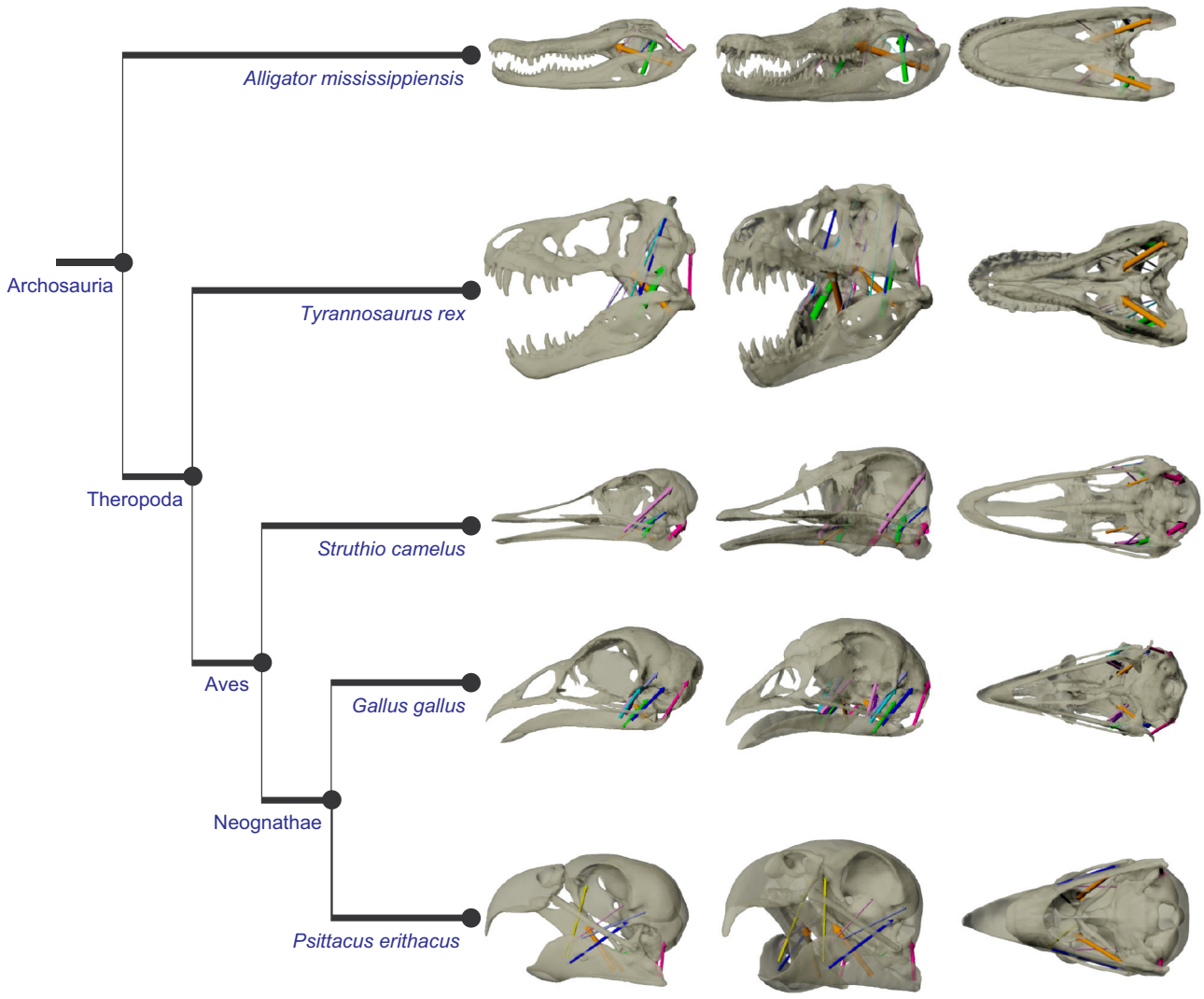

Fig. 1. Phylogenetic tree showing archosaurs used in case studies presented in this paper. Columns show skulls presented in this study in (L to R) left lateral, left oblique and ventral views.

when necessary (Baumel et al., 1993; Holliday and Witmer, 2007; Holliday, 2009).

Modeling muscle orientation and force

Muscle resultants were computed from physiological cross-sectional area (PCSA) estimations, areas of muscle attachments and the centroids of the attachments (Fig. 3C). Physiological cross-sectional areas of muscles were determined by physical dissection or extant phylogenetic bracketing of taxa, as in *T. rex* (Witmer, 1995; Sellers et al., 2017; Cost et al., 2020). Muscle parameters such as pennation angles were estimated as falling within known ranges for alligators and birds, and osteological correlates of representative fossils informed PCSA estimates in *T. rex* (Cost et al., 2020). Three-dimensional muscle orientations were calculated from the centroid of one attachment to the centroid of the opposite attachment. The centroids and muscle areas were

Table 1. Scan parameters of specimens used in this study

Taxon	Specimen number	Scan resolution (μm)	Skull length (mm)	Scanner used
Alligator mississippiensis	MUVC AL 031	0.083^3	48	Siemens INVEON164 SPECT/CT
	MUVC AL 622	$0.160^2 \times 0.5$	99	GE LightSpeed VCT
	MUVC AL 612	$0.250^2 \times 0.5$	203	GE LightSpeed VCT
	MUVC AL 024	$0.430^2 \times 0.625$	269	GE LightSpeed VCT
	MUVC AL 700	$0.510^2 \times 0.5$	333	GE LightSpeed VCT
	MUVC AL 008	0.570^3	454	Siemens Somatom Definition Scanner
Gallus gallus	MUVC AV 003	0.092^3	68	Siemens INVEON164 SPECT/CT
Struthio camelus	OUVC10659	$0.036^2 \times 0.1$	184	General Electric LightSpeed Ultra Multislice
Psittacus erithacus	MUVC AV 042	0.063^3	66	Siemens INVEON164 SPECT/CT
	MUVC AV 092	0.063^3	66	Zeiss Xradia 510 Versa 3D
Tyrannosaurus rex	BHI 3033	0.625^3	1470	General Electric LightSpeed Ultra Multislice

Journal of Experimental Biology (2022) 225, jeb243216. doi:10.1242/jeb.243216

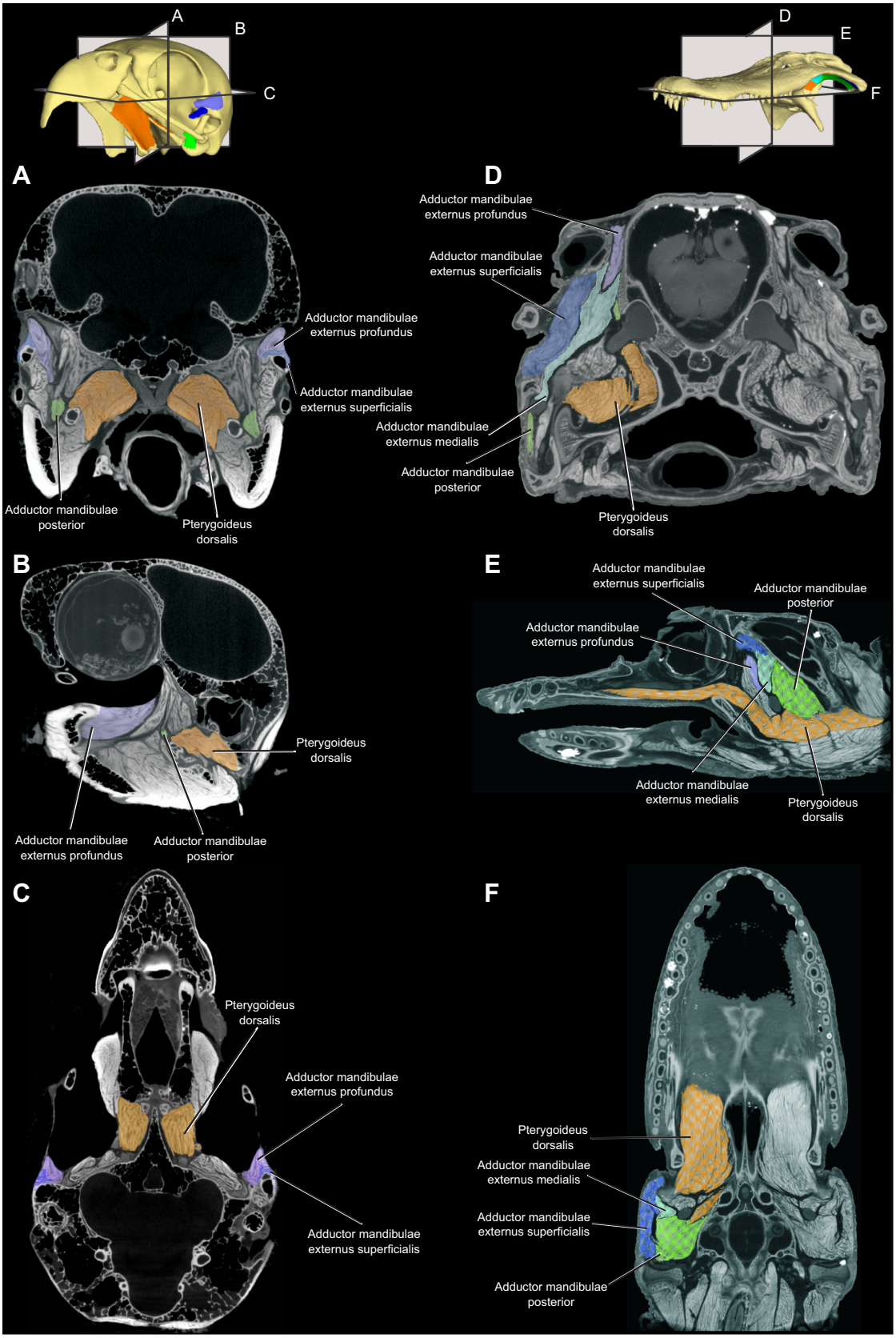

Fig. 2. Muscles pictured *in situ* in diffusible iodine contrast-enhanced computed tomography (DiceCT). (A–C) Grey parrot (*Psittacus erithacus*; MUVCAV092) and (D–E) alligator (*Alligator mississippiensis*; MUVCAL031) are used to show muscles of the cranium discussed in this study. Muscles include m. adductor mandibulae externus superficialis (mAMES), m. adductor mandibulae externus medialis (mAMEM), m. adductor mandibulae externus profundus (mAMEP), m. adductor mandibulae posterior (mAMP) and m. pterygoideus dorsalis (mPTd). Images are shown in axial (A,D), sagittal (B,E), and transverse (C,F) planes; the legend for the planes in each taxon is shown at the top.

Journal of Experimental Biology (2022) 225, jeb243216. doi:10.1242/jeb.243216

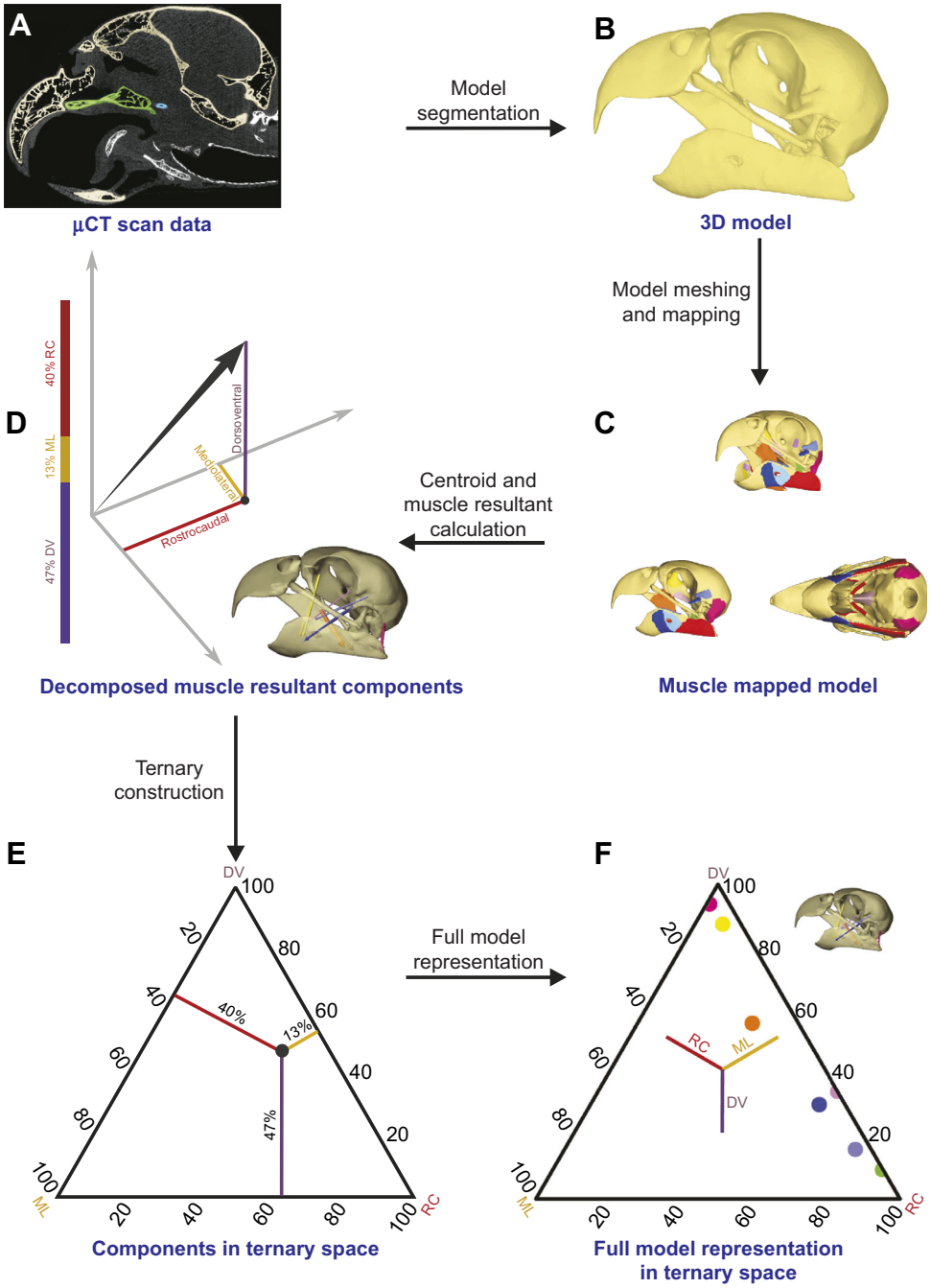

Fig. 3. Illustrated description of ternary diagram construction. (A) Computed tomography (CT), or microcomputed tomography (µCT) where appropriate, data is collected. Data are then segmented (B) and reconstructed, smoothed, and meshed to create a finite element model (FEM; C). Muscles are attached to the finished FEM and the coordinates of the centroids of attachment areas are determined. The centroids are employed to determine a muscle resultant vector between the two attachment centroids of a muscle; one on the mandible, the other on the cranium. (D) The resultant vectors are then decomposed into rostrocaudal, mediolateral and dorsoventral components. The resultant vector can be described in terms of what proportion of the total each component accounts for, in which the dorsoventral component accounts for 47% of the resultant vector, the mediolateral component accounts for 13% and the rostrocaudal component accounts for 40%. (E) The resulting point in space is then plotted on a ternary diagram using the components detailed above. (F) The final product of this process results in multiple points representing the 3D orientations of muscle resultants plotted in 2D space that enable researchers to view and appreciate the region in 3D space which muscles occupy.

calculated from stereolithographic (STL) models using the script Area_Centroid_From_STL (Davis et al., 2010; Santana et al., 2010).

Data transformation and how to read ternary diagrams

Ternary diagrams are used to represent three-variable systems in which the sum of the variables is a constant. Here, the three relative positional components (x, y, z) of a vector sum to 1, representing the contribution of each orthogonal direction to the total vector. To calculate relative contributions for a muscle vector, a 3D vector representing coordinates of a muscle's origin (x_{or}, y_{or}, z_{or}) and insertion (x_{ins}, y_{ins}, z_{ins}) is first calculated by subtracting origin coordinates from insertion coordinates (Eqn 1):

$$(x_0, y_0, z_0) = (x_{ins} - x_{or}, y_{ins} - y_{or}, z_{ins} - z_{or}). \quad (1)$$

The resulting vector is normalized to a unit vector by dividing each element by the vector's magnitude (Eqn 2):

$$(x, y, z) = \left(\frac{x_0}{\sqrt{x_o^2 + y_0^2 + z_0^2}}, \frac{y_0}{\sqrt{x_o^2 + y_0^2 + z_0^2}}, \frac{z_0}{\sqrt{x_o^2 + y_0^2 + z_0^2}} \right). \quad (2)$$

The relative proportions of (x, y, z) are then calculated as (Eqn 3):

$$(x', y', z') = \left(\frac{x^2}{x^2 + y^2 + z^2}, \frac{y^2}{x^2 + y^2 + z^2}, \frac{z^2}{x^2 + y^2 + z^2} \right). \quad (3)$$

These relative proportions (x', y', z'), which sum to 1, represent the contributions of the mediolateral (x'), dorsoventral (y'), and rostrocaudal (z') components of each muscle's 3D orientation. For example, consider the vector **v** shown in Fig. 3D. This vector represents an arbitrary muscle with its origin at (3.6, 6.9, 6.3) and its

Journal of Experimental Biology (2022) 225, jeb243216. doi:10.1242/jeb.243216

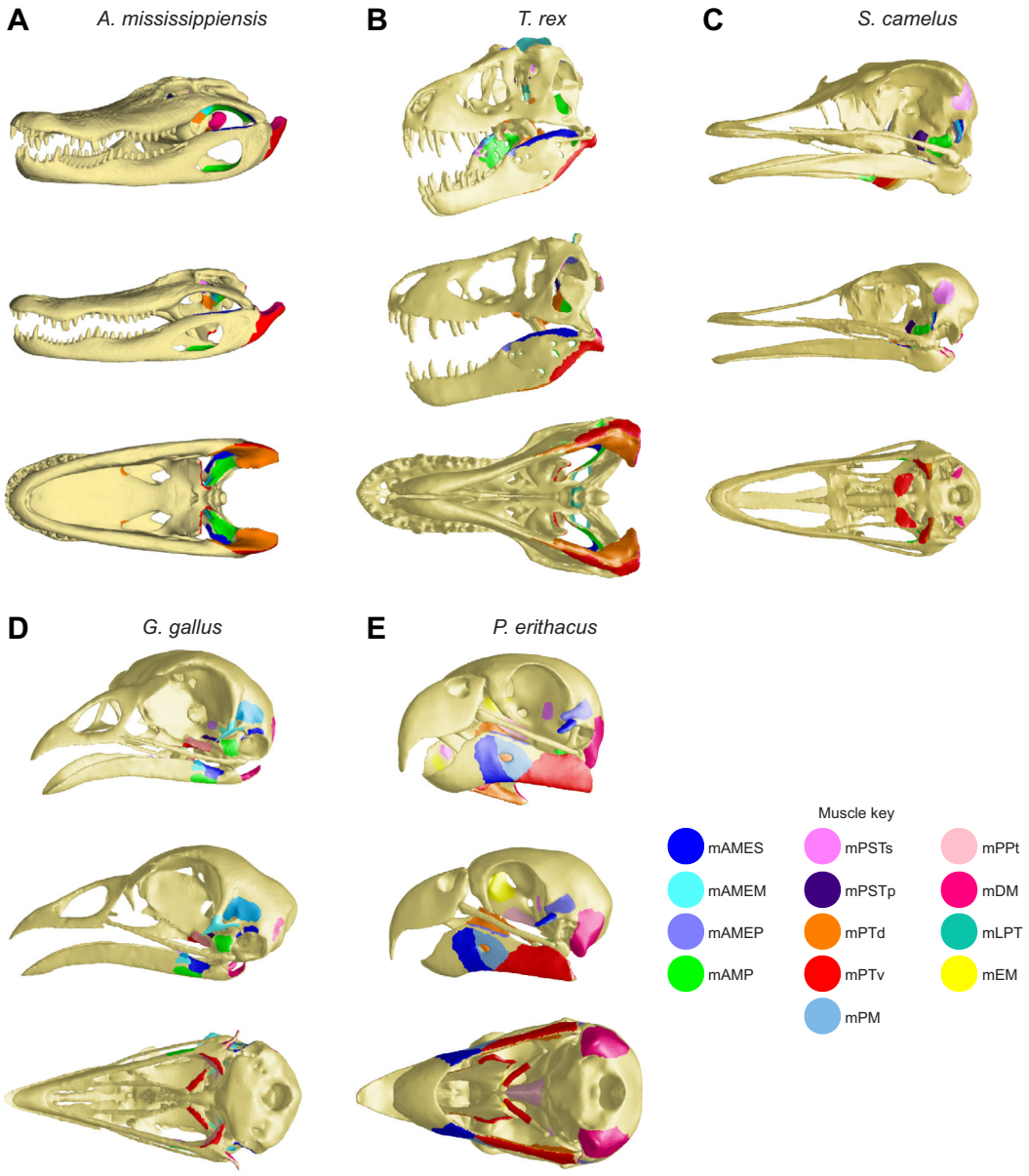

Fig. 4. Muscle maps of models used to analyze muscle resultants in this study. Oblique (top), left lateral (middle), and ventral (bottom) views of muscle mapped models are shown. Models are arranged taxonomically: (A) *Alligator mississippiensis*, (B) *Tyrannosaurus rex*, (C) *Struthio camelus*, (D) *Gallus gallus* and (E) *Psittacus erithacus*. Models are hosted on OSF: https://osf.io/E3V7U/. mAMES, m. adductor mandibulae externus superficialis; mAMEM, m. adductor mandibulae externus medialis; mAMEP, m. adductor mandibulae externus profundus; mAMP, m. adductor mandibulae posterior; mPSTs, m. pseudotemporalis superficialis; mPSTp, m. pseudotemporalis profundus; mPTd, m. pterygoideus dorsalis; mPTv, m. pterygoideus ventralis; mPM, m. pseudomasseter; mPPt, m. protractor pterygoideus; mDM, m. depressor mandibulae; mLPT, m. levator pterygoideus; mEM, m. ethmomandibularis.

insertion at (1.1, 2.1, 1.9). The calculation of **v** from muscle attachment centroids is shown in Eqn 4:

$$(1.1-3.6,\ 2.1-6.9,\ 1.9-6.3)=(-2.5,\ -4.8,\ -4.4). \quad (4)$$

The unit vector of **v** is calculated in Eqn 5:

$$\left(\frac{-2.5}{\sqrt{(-2.5)^2+(-4.8)^2+(-4.4)^2}},\frac{-4.8}{\sqrt{(-2.5)^2+(-4.8)^2+(-4.4)^2}},\frac{-4.4}{\sqrt{(-2.5)^2+(-4.8)^2+(-4.4)^2}}\right)=(-0.36,\ -0.69,\ -0.63). \quad (5)$$

The relative proportions of (x, y, z) are then calculated in Eqn 6:

$$(x',y',z')=\left(\frac{(-2.5)^2}{(-2.5)^2+(-4.8)^2+(-4.4)^2},\frac{(-4.8)^2}{(-2.5)^2+(-4.8)^2+(-4.4)^2},\frac{(-4.4)^2}{(-2.5)^2+(-4.8)^2+(-4.4)^2}\right)=(0.13,\ 0.47,\ 0.40). \quad (6)$$

Fig. 3E shows a ternary diagram with a point representing this vector. The lengths of the colored lines are proportional to the

Journal of Experimental Biology (2022) 225, jeb243216. doi:10.1242/jeb.243216

proportions of the vector. This vector represents a muscle with a low mediolateral component; as such, the point is far from the corner labeled 'ML' (Fig. 3E, bottom left) and the corresponding yellow line is short. The dorsoventral and rostrocaudal components are several times that of the mediolateral component, and the dorsoventral component is a bit higher, so the point is slightly closer to the corner labeled 'DV' (top) than to the corner labeled 'RC' (bottom-right). Ternary diagrams were used to represent the component vectors of all of the jaw muscles in two dimensions, with size of the point scaled to each muscle's force (Fig. 3F). All calculations and plots were solved and created, respectively, in R (v. 3.5.1; https://www.r-project.org/) using the custom-written and freely available R package MuscleTernary (https://github.com/Middleton-Lab/MuscleTernary), which extends the R packages ggtern (v. 3.0.0; Hamilton and Ferry, 2018) and ggplot2 (v. 3.1.1; https://CRAN.R-project.org/package=ggplot2).

Case studies

We demonstrate this approach using three case studies that explore jaw muscle resultants over three scales of time: during biting, through ontogeny, and across phylogeny. To visualize changes in muscle orientation between high and low gapes during an orthally biting feeding behavior, we plotted muscle parameters in ternary space for two specimens (1 juvenile, 1 adult) of *A. mississippiensis* by manipulating the mandibles to 5 deg and 30 deg of gape. A gape of 5 deg allows the animal to exert near its peak bite force, and at 30 deg, the jaws are at more extreme separation. Ternary coordinates for these models can be found in Table S1. To visualize changes in muscle orientation through ontogeny, we plotted the muscle parameters in ternary space for individuals of *A. mississippiensis* ranging from juvenile (head length=4.9 cm) to adult (head length=45.4 cm). Ternary coordinates for these models can be found in Table S2. To visualize changes in muscle orientation across a phylogeny, three avian taxa and one non-avian dinosaur were plotted in ternary space and the patterns of muscle orientation were analyzed and their differences described. Non-avian theropod and avian taxa were constructed with a gape of 20 deg. This value was chosen because it was the lowest gape determined to be of optimal performance in theropods by Lautenschlager (2015). Muscle resultants were plotted in ternary space (Table S3) to show patterns within the dinosaur lineage.

RESULTS

Behavior: jaw muscle resultants and gape in *Alligator mississippiensis*

As gape decreases in *A. mississippiensis*, muscle insertion points on the lower jaw rotate caudoventrally and cause most muscles to exchange dorsoventral for rostrocaudal orientations (Fig. 5). If the jaws rotate symmetrically about the two quadratoarticular joints in an orthal jaw closing bite, the mediolateral component of most jaw closing muscles necessarily increases. The dorsoventral components of certain muscles (mAMES, mAMEM, mAMEP and mAMP) are reoriented mediolaterally as gape decreases during a bite. In ternary space, this is represented by points moving away from the top of the triangle and toward the bottom left corner. The pseudotemporalis muscles mPSTs and mPSTp are reoriented more rostrocaudally and dorsoventrally, respectively, at a low gape. The resultant of mPTd decreased rostrocaudally and increased mediolaterally and dorsoventrally as the gape decreased. In this instance, the point in ternary space moves away from the bottom right corner and toward the top and left, settling in the middle area of the ternary plot (Fig. 5). The jaw opening muscle mDM becomes more dorsoventrally oriented as the jaw is closed and does not reorient mediolaterally.

Ontogeny: jaw muscle resultants and growth in *A. mississippiensis*

Overall, temporal muscles in individual alligators become less dorsoventral throughout ontogeny (Fig. 6). A rostrocaudal increase in muscle orientation is most appreciable in the external temporal muscles (mAMES, mAMEP and mAMEM). Rostrocaudal increases in temporal muscle orientations move the corresponding point in ternary space toward the lower right region of the ternary

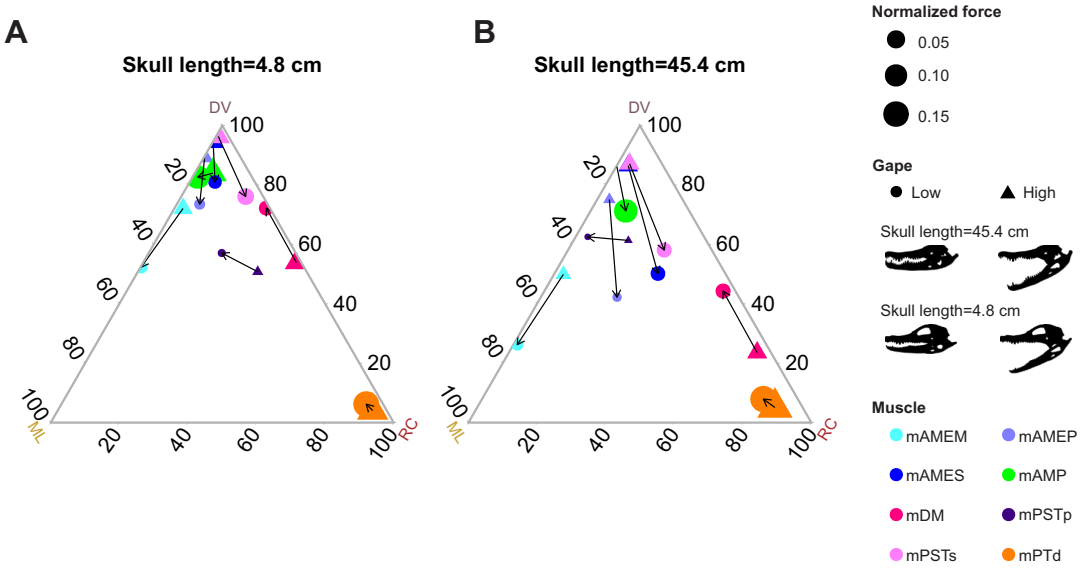

Fig. 5. Changes in muscle orientations during a gape cycle in *Alligator mississippiensis* (MUVCAL008 and MUVCAL031). Orientations of muscles at 30 deg and 5 deg of gape (high to low gape) are represented in ternary space for skull lengths of (A) 4.8 cm and (B) 45.4 cm. Arrows point from orientations at high gape (triangles) to the orientation of the corresponding muscle at low gape (circles). For both specimens, the normalized force of each muscle represents the force of that muscle as a proportion of total jaw muscle force. Changes in orientation are most appreciable in the temporal muscle complex (mAMES, mAMEM, mAMEM), and mAMP and mDM. The mPTd undergoes little to no change in orientation during a gape cycle. Muscle abbreviations as in Fig. 4.

Journal of Experimental Biology (2022) 225, jeb243216. doi:10.1242/jeb.243216

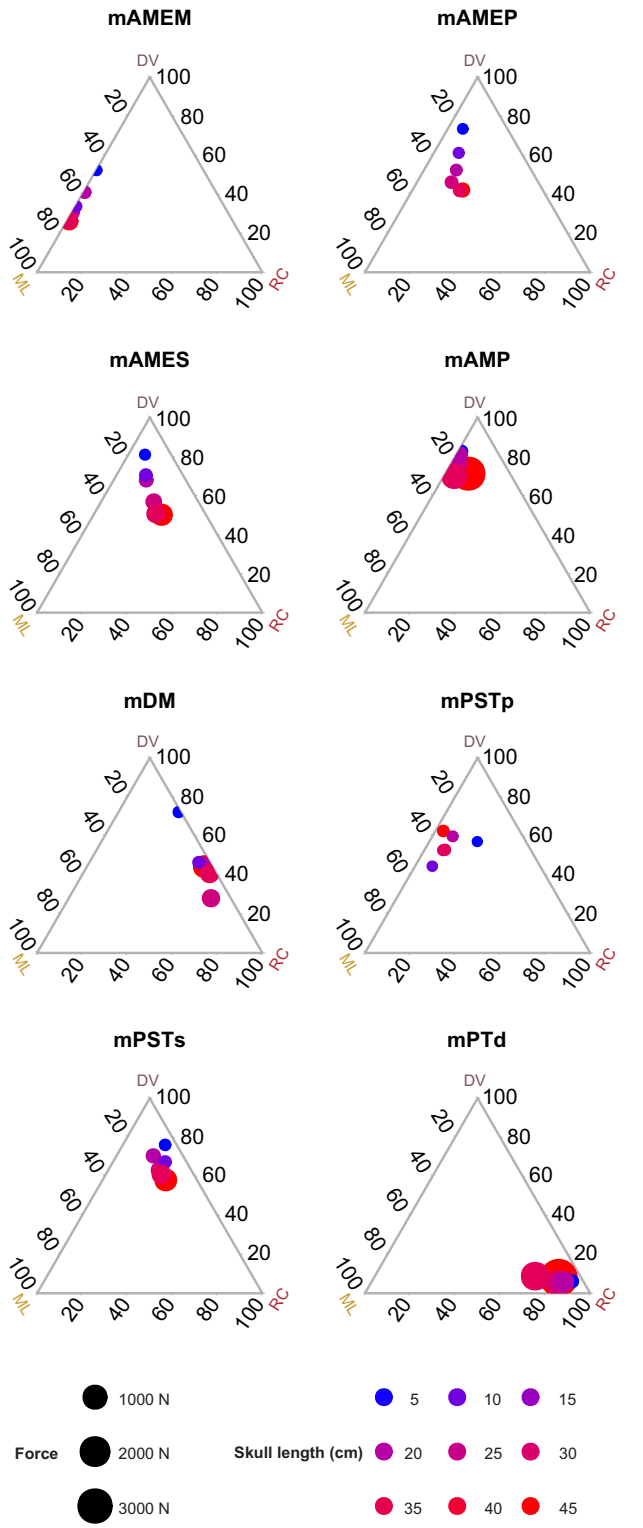

Fig. 6. Ontogenetic changes in muscle orientation in *A. mississippiensis* (MUVCAL008, MUVCAL024, MUVCAL031, MUVCAL612, MUVCAL622 and MUVCAL700). Changes over a growth series of *A. mississippiensis* are represented in ternary space with points representing muscle belly orientation. Points are depicted ranging from lighter to darker red colors which represent smaller to larger individuals, respectively. Orientations of temporal muscles in *A. mississippiensis* become more rostrocaudal or mediolateral as alligators mature and become larger. Musculus pterygoideus dorsalis does not follow a linear path throughout ontogeny, but largely retains a highly rostrocaudal orientation as individuals grow from hatchling to adult. Muscle abbreviations as in Fig. 4.

plot. The muscle mPSTs increases the mediolateral and rostrocaudal components but still retains a highly dorsoventral orientation whereas mPSTp increases the dorsoventral component and loses some rostrocaudal orientation. The other large adductor muscle, mAMP, experiences a slight ontogenetic decrease in its dorsoventral component and corresponding increase in its rostrocaudal component. The point representing mAMP therefore moves away from the top of the ternary plot and closer to the bottom right corner as animals increase in size. However, this change is not large, and mAMP largely retains its juvenile orientation overall as an adult. Musculus pterygoideus dorsalis (mPTd) retains and increases its rostrocaudal orientation; however, the changes associated with ontogenetic development are not as great as in the temporal muscles. The point for mPTd moves farther into the bottom right corner of the ternary diagram in this instance. The least change over ontogeny is seen in mAMP and mPTd. These two muscles retain large dorsoventral (mAMP) and rostrocaudal (mPTd) orientations. Musculus depressor mandibulae (mDM) does not change its orientation throughout ontogeny, remaining nearly equally dorsoventrally (≈47.5%) and rostrocaudally (≈47.5%) oriented with very small mediolateral components (<5%).

Phylogenetic patterns of jaw muscle resultants

The effects of evolutionary changes on jaw muscle resultants are illustrated here in ternary space using a non-avian dinosaur (*T. rex*; Fig. 7B) and three avians (*S. camelus*, *G. gallus* and *P. erithacus*; Fig. 7C–E); adult alligator is also presented here as an outgroup (Fig. 7A). The temporal muscles (mAMEP, mAMES, mAMEM, mPSTs, mPSTp) as well as mAMP of *T. rex* are largely dorsoventrally oriented (Fig. 7B). The mPTd of *T. rex* is mixed, with contributions from all directions causing the resultant to reside nearer the center of the plot. In the paleognath *S. camelus* (Fig. 7C), the temporal muscles are almost entirely rostrocaudally oriented, but all possess dorsoventral aspects as well. Unique to *S. camelus* among other avian taxa sampled here, the resultant for mPSTp is centrally located in ternary space. The mPTd of *S. camelus* is largely rostrocaudal with a small dorsoventral component.

The temporal and pterygoideus muscles of the neognath *G. gallus* are largely rostrocaudally oriented but also possess dorsoventral components relatively greater than those observed in *S. camelus* (Fig. 7D). The orientations of mAMEP, mAMES, and mAMP possess very limited mediolateral components whereas mAMEM, mPSTs, and mPSTp exhibit more dorsoventral orientation at the expense of rostrocaudal orientation. This is shown through the resultants residing in the upper central area of the ternary. The mPTd possesses the most evenly distributed orientation in *G. gallus*. The muscle orientations of *P. erithacus*, another neognath, are different from *G. gallus* (Fig. 7E). *Psittacus* possesses rostrocaudally oriented temporal muscles but also exhibits more mediolateral muscle resultant components. Additionally, *P. erithacus* possesses a parrot-specific muscle mEM which is extremely dorsoventrally oriented. Musculus depressor mandibulae is highly dorsoventral across all avian taxa sampled. A small mediolateral component is also present. The muscle orientations of the temporal muscles contain appreciable mediolateral components, especially in mAMES and mAMEP. In *P. erithacus*, mPTd is highly dorsoventrally and mediolaterally oriented. The rostrocaudal component of mPTd in *P. erithacus* is relatively comparable to *G. gallus* and *T. rex* as well.

Muscle orientation in hard biting taxa

This case study considers the hardest biting fossil and extant taxa (*T. rex* and *A. mississippiensis*). A third taxon, *P. erithacus*, also

Journal of Experimental Biology (2022) 225, jeb243216. doi:10.1242/jeb.243216

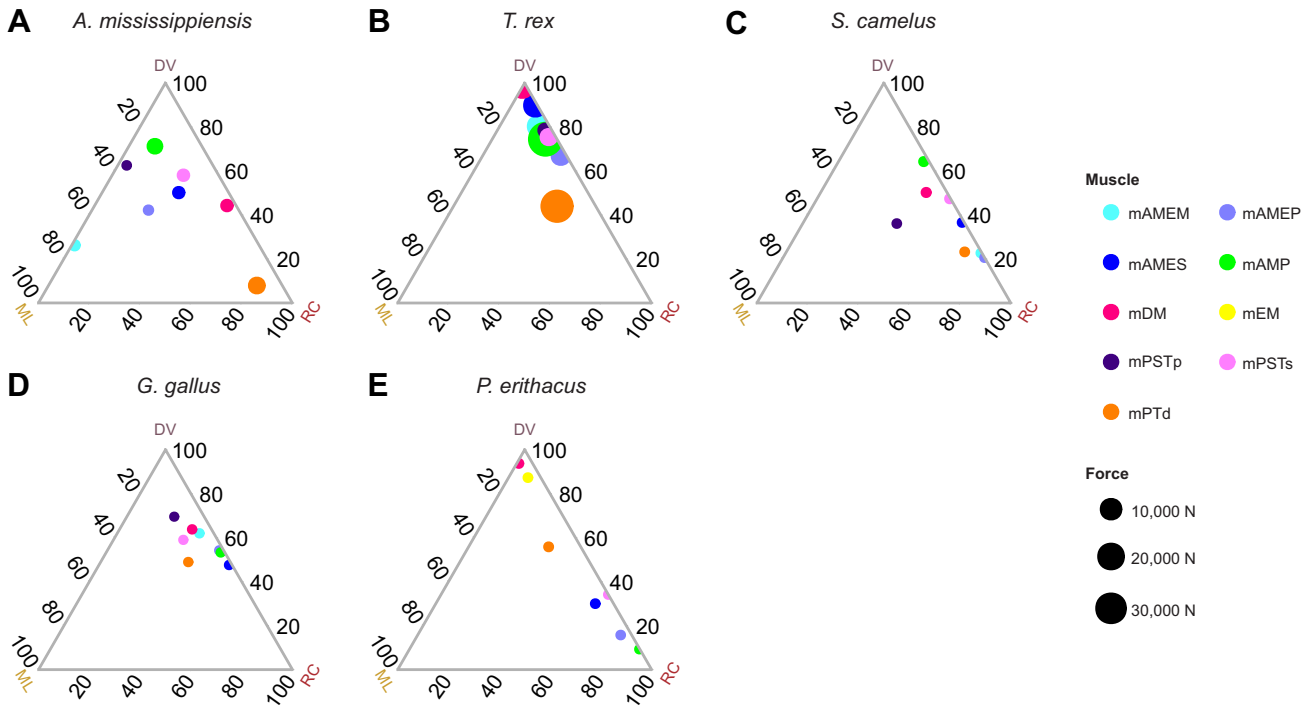

Fig. 7. Diversity in jaw muscle orientation among a non-avian theropod dinosaur (*Tyrannosaurus rex* BHI 3033) and avian theropod dinosaurs (*Struthio camelus* OUVC10659; *Gallus gallus* MUVCAV003; *Psittacus erithacus* MUVCAV042). (A) Adult *A. mississippiensis* is retained as an outgroup and for comparison of hard-biting taxa. (B) *T. rex* temporal muscles are highly dorsoventrally oriented, whereas avian temporal muscles are generally more rostrocaudally oriented. The muscle mPTd retains a mainly rostrocaudal orientation in *S. camelus* (C), but is appreciably mediolateral in *G. gallus* (D), *P. erithacus* (E) and *T. rex* (B). Muscle abbreviations as in Fig. 4.

produces relatively high bite forces compared with other birds (e.g. Sustaita and Hertel, 2010; Carril et al., 2015). The three taxa produce high bite forces with different cranial configurations: *A. mississippiensis* possesses a dorsoventrally short, mediolaterally wide skull whereas *T. rex* and *P. erithacus* both possess dorsoventrally tall and mediolaterally wide skulls.

Despite possessing a dorsoventrally short skull, *A. mississippiensis* temporal muscles possess appreciable dorsoventral and mediolateral components (Fig. 7A). The temporal muscles are relatively weaker than mPTd and mAMP (see Figs 5 and 6), and these two muscles possess extensive rostrocaudal and dorsoventral components, respectively. The force of mPTd and mAMP together constitute approximately 35% of the total bite force produced by *A. mississippiensis* (Sellers et al., 2017). *T. rex* and *P. erithacus* also both exhibit very few mediolateral muscle components except in mPTd (Fig. 7B,E). The temporal muscles are largely dorsoventral and rostrocaudal in *T. rex* and *P. erithacus*, respectively. The exceptions to large rostrocaudal components in *P. erithacus* are in mPTd, which exhibits a highly dorsoventral and appreciable mediolateral orientation and the extremely dorsoventral mEM (Fig. 7E). In *T. rex*, the mPTd has a greater rostrocaudal orientation than any other muscle. The dorsoventral components of mPTd are relatively greater than the dorsoventral components of mPTd in *P. erithacus* compared with those of *T. rex*.

DISCUSSION

Behavior: jaw muscle resultants and gape in *A. mississippiensis*

Movement of the mandibles with respect to the cranium during feeding translates muscle insertions relative to their origins, leading to differing muscle orientations at different gape angles. As some muscle orientations are less effective at producing a given mandibular movement (e.g. jaw adduction), the gape angle can influence a system's ability to generate forces in a given direction (e.g. Eng et al., 2009; Lautenschlager, 2015). The results of the gape case study in *A. mississippiensis* confirm the general pattern that jaw closing muscles studied here increased their mediolateral components as gape decreased. Increases in mediolateral components decreases the relative vertical force that mAMEM contributes to bite force whereas mPTd relatively increases its contributions to bite force because it is not reoriented mediolaterally.

Additionally, in both the juvenile and adult, mAMP retained much of its dorsoventral components (more in the juvenile than the adult). As gape decreased, the dorsoventral component of mPTd increased. Sellers et al. (2017) determined that over one-third of total bite force is derived from the individual muscle forces of mPTd and mAMP. Retention of the dorsoventral components of the muscles enables these muscles to maintain high vertical bite forces even at low gapes. These results show that the decrease in dorsoventral components in many of the temporal muscles is potentially compensated for at low gapes by the increase in mPTd dorsoventral orientation.

Ontogeny: jaw muscle resultants and growth in *A. mississippiensis*

Morphological changes of the skull are known to impact the feeding performance and ecology of the alligator (Erickson et al., 2003; Sellers et al., 2017). These morphological changes manifest as the skulls of alligators flatten considerably during their thousand-fold ontogenetic increase in body size (Dodson, 1975; Busbey, 1997; Monteiro et al., 1997; Brochu, 2001; Piras et al., 2014). Compared

with the rest of the skull, the braincase and skull roof of adult alligators are more mediolaterally positioned relative to the jaw joints and mandibles than the same structures in juveniles (Mook, 1921a,b; Iordansky, 1973; Monteiro et al., 1997), which displaces the cranial attachments of temporal muscles mediolaterally. The ramus of the quadrate also shifts caudolaterally (Mook, 1921a,b; Iordansky, 1973; Monteiro et al., 1997), which gives some muscles a more rostrocaudal orientation in addition to the mediolateral dimension. As expected, shape changes in the skull cause a range of shifts in the resultants of some jaw muscles like the temporal muscles. However, changes over ontogeny are less evident in the pterygoideus muscles. Similarities in mAMP and mPTd throughout ontogeny likely reflect the integral roles that these two muscles play in increasing the bite force of alligators throughout the gape cycle regardless of specimen age.

Phylogenetic patterns of jaw muscle resultants

The phylogenetic results are presented as a small-scale proof-of-concept that could be elaborated upon in future comparative studies across Archosauria. This study shows that jaw muscle resultants vary considerably across taxa but that ternary plots offer new ways to visually compare these differences and make predictions about evolutionary transformations, such as those along the lines to extant birds from non-avian theropod dinosaurs. Not only does the increased encephalization and expanded braincase (Balanoff et al., 2016; Fabbri et al., 2017) likely alter resultants of temporal muscles across the clade, but changes in the linkages and shapes of the palatal elements (Huxley, 1867; Bock, 1964, 1999; Gussekloo and Zweers, 1999) and the origin of avian-style powered kinesis likely altered the organization of palatal muscles.

Muscle resultants in *T. rex* are highly dorsoventrally oriented and possess few mediolateral or rostrocaudal components. Although not tested, this muscle morphology seems similar to what we envision in many other non-avian dinosaurs like *Allosaurus* spp. Birds, however, exhibit muscle resultants that are more rostrocaudal and, in neognathe taxa, possess some mediolateral components in the non-temporal mPTd. In *G. gallus* there are also mediolateral components evident in mAMEM, mPSTs, and mPSTp. Holliday (2006) and Holliday and Witmer (2008) described the lateral expansion of the braincase and reduction of the temporal region in birds as major features driving the evolution of the feeding apparatus of birds. This combination of braincase inflation and kinesis requires that the temporal muscles not only have a more dorsoventral than mediolateral orientation, but also more rostrocaudally oriented forces. This is driven by the derived propulsive nature of kinesis present in neognathe birds, particularly parrots as shown here, relative to other avian taxa. The translation of muscle resultants to a more rostrocaudal orientation is likely related to the evolution of powered, propulsive cranial kinesis in neognathe birds.

Differences between paleognathe and neognathe birds are subtler than those between sampled non-avian and avian theropods. The temporal muscles, though, are fairly similar in their rostrocaudal orientations. The trends described in this proof-of-concept study are shown with a small sample size; however, we are confident that an increase in sample size will only serve to bolster these trends in the dinosaur to bird evolutionary line.

Muscle orientation in hard biting taxa

Our final case study indicates that species that can generate high bite forces can do so using variable muscle resultant orientations. The ternary diagrams in this section also illustrate how ecomorphs might converge in function despite disparate cranial shapes. Numerous vertebrate species have evolved increased bite forces in order to dispatch prey (e.g. *A. mississippiensis*, *T. rex*) or to husk tough food items (e.g. *P. erithacus*), and in these cases, we expect the skulls to have increased vertical components of jaw muscle resultants, as vertical forces are more optimally in line with orthal forces driven into food items.

The highly vertical muscle orientations found here in diverse adductor muscles of *A. mississippiensis* (mAMP), *T. rex* (mAMEP, mAMEM, mAMES, mPSTs, mPSTp and mAMP) and *P. erithacus* (mPTd, mEM) show that hard biting archosaurs employ different biomechanical strategies to generate relatively high bite forces. As in gape (Fig. 5), mPTd in *A. mississippiensis* increases its dorsoventral component as gape decreases, contributing a larger dorsoventral component at low gape. *A. mississippiensis* produces high bite forces using one highly dorsoventrally oriented muscle (mAMP) and one rostrocaudally oriented muscle (mPTd) that increases its dorsoventral orientation at low gapes. This reorientation of mPTd appears to compensate for the decreases in dorsoventral orientations in other muscles.

Dorsoventral bite force production of *T. rex* is largely the result of the temporal muscles (mAMEP, mAMEM, mAMES, mPSTs, mPSTp and mAMP). This dorsoventral orientation of high force producing muscles is in line with expectations for hard-biting taxa mentioned previously. *P. erithacus*, however, employs a pterygoideus muscle (mPTd) and a parrot-specific muscle (mEM) to produce high bite forces. The temporal muscles of *P. erithacus* contribute less overall force to the bite force of the animal as these muscles (mAMEP, mAMES, and mAMP) are oriented more rostrocaudally.

Conclusions

Ternary diagrams are a powerful means of conveying complex muscle orientation data in comparative contexts across behavior, ontogeny, and phylogeny. All of our case studies provide solid proof-of-concept work that lays a solid foundation for future studies using ternary diagrams to visualize and interpret complex biomechanical data and concepts. We identify trends in muscle orientation changes across gape in juvenile and adult specimens as well as ontogenetic changes within the same lineage (*A. mississippiensis*). Decreases in gape during biting in *A. mississippiensis* change the resultant orientation of muscles in both juvenile and adult specimens to a more mediolateral orientation. Over ontogeny in *A. mississippiensis*, however, the orientations of the muscles shift rostrocaudally and mediolaterally. In the dinosaur-avian lineage, muscle resultant orientations were shifted rostrocaudally and mediolaterally along the dinosaur-to-bird axis. More dinosaur taxa are needed to better illustrate this pattern. This case study shows that future comparison studies across lineages of extinct and extant taxa can be conducted in a meaningful way that incorporates complex and informative 2D visualizations of 3D muscle systems. Finally, we showed that among archosaurs, hard-biting taxa generate high bite forces using disparate arrangements of jaw muscles. Data like these will enable us to follow the evolutionary changes that resulted in different anatomical solutions to functional demands. Future studies can make use of these types of ecomorphological variables to study the convergence of bones and muscles across guilds of animals. Studies that estimate ancestral states and evaluate the tempo of adaptive radiations of animals that modify the feeding apparatus (e.g. cichlids) could also benefit from using ternary diagrams to present data and results.

Acknowledgements
We thank M. Scott Echols, Lawrence Witmer, and Ruth Elsey and the staff at the Rockefeller Wildlife Refuge for specimens. We thank Julian Davis, Stephen Gatesy, Emily Rayfield, Ryan Ridgely and Lawrence Witmer for discussions throughout the development of this paper. We thank the Truman VA Biomolecular Imaging Center (Columbia, MO), University Hospital Department of Radiology (University of Missouri, Columbia, MO), School of Veterinary Medicine (University of Missouri, Columbia, MO), Geological Sciences X-ray Microanalysis Core (University of Missouri, Columbia, MO), and OhioHealth O'Bleness Hospital (Athens, OH) for scanning specimens used in this study. We are grateful for the input of two anonymous reviewers whose thoughtful suggestions improved the manuscript.

Competing interests
The authors declare no competing or financial interests.

Author contributions
Conceptualization: I.N.C., K.C.S., K.M.M., C.M.H.; Methodology: I.N.C., K.C.S., K.M.M.; Software: I.N.C., K.C.S., K.M.M.; Validation: I.N.C., K.C.S., R.E.R., A.T.S., K.M.M.; Formal analysis: I.N.C., K.C.S., C.M.H.; Investigation: I.N.C., K.C.S., R.E.R., A.T.S.; Resources: K.M.M., C.M.H.; Data curation: K.M.M.; Writing - original draft: I.N.C., K.C.S., K.M.M.; Writing - review & editing: I.N.C., K.C.S., K.M.M., C.M.H.; Visualization: I.N.C., K.C.S., R.E.R., A.T.S., K.M.M., C.M.H.; Supervision: C.M.H.; Project administration: C.M.H.; Funding acquisition: K.M.M., C.M.H.

Funding
This work was supported by the National Science Foundation [IOS-1457319 to C.M.H. and K.M.M., E.A.R. 1631684 to C.M.H.]; University of Missouri Research Board; University of Missouri Research Council; and University of Missouri Department of Pathology and Anatomical Sciences.

Data availability
3D Vector models and other raw data are hosted on the Open Science Framework: doi:10.17605/OSF.IO/E3V7U.

References

Arnold, K., Bordoli, L., Kopp, J. and Schwede, T. (2006). The SWISS-MODEL workspace: a web-based environment for protein structure homology modelling. *Bioinformatics* **22**, 195-201. doi:10.1093/bioinformatics/bti770
Baier, D. B., Gatesy, S. M. and Dial, K. P. (2013). Three-dimensional, high-resolution skeletal kinematics of the avian wing and shoulder during ascending flapping flight and uphill flap-running. *PLoS ONE* **8**, e63982. doi:10.1371/journal.pone.0063982
Balanoff, A. M., Smaers, J. B. and Turner, A. H. (2016). Brain modularity across the theropod-bird transition: testing the influence of flight on neuroanatomical variation. *J. Anat.* **229**, 204-214. doi:10.1111/joa.12403
Bates, K. T. and Falkingham, P. L. (2018). The importance of muscle architecture in biomechanical reconstructions of extinct animals: a case study using *Tyrannosaurus rex*. *J. Anat.* **233**, 625-635. doi:10.1111/joa.12874
Baumel, J. J., King, A. S., Breazile, J. E., Evans, H. E. and Vanden Berge, J. C. (1993). *Nomina Anatomica Avium II.* Publications of the Nuttall Ornithology Club (USA) no. 23.
Bimber, O., Gatesy, S. M., Witmer, L. M., Raskar, R. and Miguel Encarnação, L. (2002). Merging fossil specimens with computer-generated information. *Computer* **35**, 25-30. doi:10.1109/MC.2002.1033024
Bock, W. J. (1964). Kinetics of the avian skull. *J. Morphol.* **114**, 1-41. doi:10.1002/jmor.1051140102
Bock, W. J. (1999). Cranial kinesis revisited. *Zool. Anz.* **238**, 27-40.
Brainerd, E. L., Baier, D. B., Gatesy, S. M., Hedrick, T. L., Metzger, K. A., Gilbert, S. L. and Crisco, J. J. (2010). X-ray reconstruction of moving morphology (XROMM): precision, accuracy and applications in comparative biomechanics research. *J. Exp. Zool. A Ecol. Genet. Physiol.* **313A**, 262-279. doi:10.1002/jez.589
Brochu, C. A. (2001). Crocodylian snouts in space and time: phylogenetic approaches toward adaptive radiation. *Am. Zool.* **41**, 564-585. doi:10.1093/icb/41.3.564
Burton, P. J. K. (1974). *Feeding and the Feeding Apparatus in Waders*. London: Trustees of the British Museum.
Busbey, A. B. (1997). Structural consequences of skull flattening in crocodilians. In *Functional Morphology in Vertebrate Paleontology* (ed. J. Thomason), pp. 173-192. Cambridge University Press.
Capano, J. G., Moritz, S., Cieri, R. L., Reveret, L. and Brainerd, E. L. (2019). Rib motions don't completely hinge on joint design: costal joint anatomy and ventilatory kinematics in a Teiid Lizard, Salvator merianae. *Integr Org Biol* **1**, oby004. doi:10.1093/iob/oby004
Carlson, K. J., Stout, D., Jashashvili, T., de Ruiter, D. J., Tafforeau, P., Carlson, K. and Berger, L. R. (2011). The endocast of MH1, Australopithecus sediba. *Science* **333**, 1402-1407. doi:10.1126/science.1203922
Carril, J., Degrange, F. J. and Tambussi, C. P. (2015). Jaw myology and bite force of the monk parakeet (Aves, Psittaciformes). *J. Anat.* **227**, 34-44. doi:10.1111/joa.12330
Cartmill, M. (1974). 2 - Pads and claws in arboreal locomotion. In *Primate Locomotion* (ed. F. A. Jenkins), pp. 45-83. Academic Press.
Cartmill, M. (1985). Climbing. In *Functional Vertebrate Morphology* (ed. M. Hildebrand, D. M. Bramble, K. F. Liem and D. B. Wake), pp. 73-88. Harvard Univ. Press.
Charles, J. P., Cappellari, O., Spence, A. J., Wells, D. J. and Hutchinson, J. R. (2016). Muscle moment arms and sensitivity analysis of a mouse hindlimb musculoskeletal model. *J. Anat.* **229**, 514-535. doi:10.1111/joa.12461
Cohen, M., Prialnik, D. and Podolak, M. (2003). A quasi-3D model for the evolution of shape and temperature distribution of comet nuclei—application to Comet 46P/Wirtanen. *New Astron.* **8**, 179-189. doi:10.1016/S1384-1076(02)00223-3
Cost, I. N., Middleton, K. M., Sellers, K. C., Echols, M. S., Witmer, L. M., Davis, J. L. and Holliday, C. M. (2020). Palatal biomechanics and its significance for cranial kinesis in Tyrannosaurus rex. *Anat. Rec.* **303**, 999-1017. doi:10.1002/ar.24219
Cuff, A. R., Bright, J. A. and Rayfield, E. J. (2015). Validation experiments on finite element models of an ostrich (*Struthio camelus*) cranium. *PeerJ* **3**, e1294. doi:10.7717/peerj.1294
Curtis, N., Jones, M. E. H., Evans, S. E., O'Higgins, P. and Fagan, M. J. (2010). Feedback control from the jaw joints during biting: an investigation of the reptile Sphenodon using multibody modelling. *J. Biomech.* **43**, 3132-3137. doi:10.1016/j.jbiomech.2010.08.001
Davis, J. L., Santana, S. E., Dumont, E. R. and Grosse, I. R. (2010). Predicting bite force in mammals: two-dimensional versus three-dimensional lever models. *J. Exp. Biol.* **213**, 1844-1851. doi:10.1242/jeb.041129
Dawson, M. M., Metzger, K. A., Baier, D. B. and Brainerd, E. L. (2011). Kinematics of the quadrate bone during feeding in mallard ducks. *J. Exp. Biol.* **214**, 2036-2046. doi:10.1242/jeb.047159
Dodson, P. (1975). Functional and ecological significance of relative growth in Alligator. *J. Zool.* **175**, 315-355. doi:10.1111/j.1469-7998.1975.tb01405.x
Du Plessis, A., Slabbert, R., Swanepoel, L. C., Els, J., Booysen, G. J., Ikram, S. and Cornelius, I. (2015). Three-dimensional model of an ancient Egyptian falcon mummy skeleton. *Rapid Prototyping J.* **21**, 368-372. doi:10.1108/RPJ-09-2013-0089
Dullemeijer, P. (1956). The functional morphology of the head of the common viper. *Arch. Neerlandaises Zool.* **11**, 387-497. doi:10.1163/036551656X00139
Dumont, E. R. and Herrel, A. (2003). The effects of gape angle and bite point on bite force in bats. *J. Exp. Biol.* **206**, 2117-2123. doi:10.1242/jeb.00375
Dumont, E. R., Piccirillo, J. and Grosse, I. R. (2005). Finite-element analysis of biting behavior and bone stress in the facial skeletons of bats. *Anat. Rec. A Discov. Mol. Cell. Evol. Biol.* **283A**, 319-330. doi:10.1002/ar.a.20165
Eng, C. M., Ward, S. R., Vinyard, C. J. and Taylor, A. B. (2009). The morphology of the masticatory apparatus facilitates muscle force production at wide jaw gapes in tree-gouging common marmosets (*Callithrix jacchus*). *J. Exp. Biol.* **212**, 4040-4055.
Erickson, G. M., Lappin, A. K. and Vliet, K. A. (2003). The ontogeny of bite-force performance in American alligator (Alligator mississippiensis). *J. Zool.* **260**, 317-327. doi:10.1017/S0952836903003819
Evans, D. C., Ridgely, R. C. and Witmer, L. M. (2009). Endocranial anatomy of lambeosaurine hadrosaurids (Dinosauria: Ornithischia): a sensorineural perspective on cranial crest function. *Anat. Rec.* **292**, 1315-1337. doi:10.1002/ar.20984
Fabbri, M., Mongiardino Koch, N., Pritchard, A. C., Hanson, M., Hoffman, E., Bever, G. S., Balanoff, A. M., Morris, Z. S., Field, D. J., Camacho, J. et al. (2017). The skull roof tracks the brain during the evolution and development of reptiles including birds. *Nat Ecol Evol* **1**, 1543-1550. doi:10.1038/s41559-017-0288-2
Figueirido, B., Tseng, Z. J. and Martín-Serra, A. (2013). Skull shape evolution in *Durophagous carnivorans*. *Evolution* **67**, 1975-1993. doi:10.1111/evo.12059
Friedrich, F. and Beutel, R. G. (2008). Micro-computer tomography and a renaissance of insect morphology. In *Developments in X-Ray Tomography VI*, p. 70781U. International Society for Optics and Photonics.
Gans, C., De Vree, F. and Carrier, D. R. (1985). Usage pattern of the complex masticatory muscles in the shingleback lizard, *Trachydosaurus rugosus*: a model for muscle placement. *Am. J. Anat.* **173**, 219-240. doi:10.1002/aja.1001730306
Gatesy, S. M. and Middleton, K. M. (1997). Bipedalism, flight, and the evolution of theropod locomotor diversity. *J. Vert. Paleontol.* **17**, 308-329. doi:10.1080/02724634.1997.10010977
Gatesy, S. M. and Middleton, K. M. (2008). Chapter 16. Skeletal adaptations for flight. In *Fins into Limbs* (ed. B. K. Hall), pp. 269-283. Chicago: University of Chicago Press.
Gignac, P. M. and Erickson, G. M. (2016). Ontogenetic bite-force modeling of *Alligator mississippiensis*: implications for dietary transitions in a large-bodied vertebrate and the evolution of crocodylian feeding. *J. Zool.* **299**, 229-238.
Greaves, W. S. (1982). A Mechanical Limitation on the Position of the Jaw Muscles of Mammals: The One-Third Rule. *J. Mammal.* **63**, 261-266. doi:10.2307/1380635

Grigg, G. and Kirshner, D. (2015). *Biology and Evolution of Crocodylians*. Csiro Publishing.
Grosse, I. R., Dumont, E. R., Coletta, C. and Tolleson, A. (2007). Techniques for modeling muscle-induced forces in finite element models of skeletal structures. *Anat. Rec.* **290**, 1069-1088. doi:10.1002/ar.20568
Gussekloo, S. W. S. and Zweers, G. A. (1999). The Paleognathous Pterygoid-Palatinum complex. A true character? *Neth. J. Zool.* **49**, 29-43. doi:10.1163/156854299X00038
Hamilton, N. E. and Ferry, M. (2018). Ggtern: ternary diagrams using ggplot2. *J. Stat. Softw.* **87**, 1-17. doi:10.18637/jss.v087.c03
Herrel, A., De Vree, F., Delheusy, V. and Gans, C. (1999). Cranial kinesis in gekkonid lizards. *J. Exp. Biol.* **202**, 3687-3698. doi:10.1242/jeb.202.24.3687
Herring, S. W. and Herring, S. E. (1974). The superficial masseter and gape in mammals. *Am. Nat.* **108**, 561-576. doi:10.1086/282934
Hoese, W. J. and Westneat, M. W. (1996). Biomechanics of cranial kinesis in birds: testing linkage models in the white-throated sparrow (*Zonotrichia albicollis*). *J. Morphol.* **227**, 305-320. doi:10.1002/(SICI)1097-4687(199603)227:3<305::AID-JMOR3>3.0.CO;2-4
Holliday, C. M. (2006). Evolution and function of the jaw musculature and adductor chamber of archosaurs (crocodilians, dinosaurs, and birds). Ohio University.
Holliday, C. M. (2009). New insights into dinosaur jaw muscle anatomy. *Anat. Rec.* **292**, 1246-1265. doi:10.1002/ar.20982
Holliday, C. M. and Witmer, L. M. (2007). Archosaur adductor chamber evolution: integration of musculoskeletal and topological criteria in jaw muscle homology. *J. Morphol.* **268**, 457-484. doi:10.1002/jmor.10524
Holliday, C. M. and Witmer, L. M. (2008). Cranial kinesis in dinosaurs: intracranial joints, protractor muscles, and their significance for cranial evolution and function in diapsids. *J. Vert. Paleontol.* **28**, 1073-1088. doi:10.1671/0272-4634-28.4.1073
Holliday, C. M., Tsai, H. P., Skiljan, R. J., George, I. D. and Pathan, S. (2013). A 3D interactive model and atlas of the jaw musculature of *Alligator mississippiensis*. *PLoS ONE* **8**, e62806. doi:10.1371/journal.pone.0062806
Huber, D. R., Dean, M. N. and Summers, A. P. (2008). Hard prey, soft jaws and the ontogeny of feeding mechanics in the spotted ratfish *Hydrolagus colliei*. *J. R. Soc. Interface* **5**, 941-953. doi:10.1098/rsif.2007.1325
Hughes, S., Wright, R. and Barry, M. (2005). Virtual reconstruction and morphological analysis of the cranium of an ancient Egyptian mummy. *Australas. Phys. Eng. Sci. Med.* **28**, 122-127. doi:10.1007/BF03178703
Hutchinson, J. R. (2004). Biomechanical modeling and sensitivity analysis of bipedal running ability. II. Extinct taxa. *J. Morphol.* **262**, 441-461. doi:10.1002/jmor.10240
Huxley, T. H. (1867). On the classification of birds, and on the taxonomic value of the modification of certain of the cranial bones. *P. Zool. Soc. Lond.*, 415-472.
Iordansky, N. N. (1973). The skull of the Crocodylia. In *Biology of the Reptilia*, Vol. 4 (ed. C. Gans and T. S. Parsons), pp. 201-262. London: Academic Press.
Kawabe, S., Shimokawa, T., Miki, H., Matsuda, S. and Endo, H. (2013). Variation in avian brain shape: relationship with size and orbital shape. *J. Anat.* **223**, 495-508. doi:10.1111/joa.12109
Keyak, J. H., Fourkas, M. G., Meagher, J. M. and Skinner, H. B. (1993). Validation of an automated method of three-dimensional finite element modelling of bone. *J. Biomed. Eng.* **15**, 505-509. doi:10.1016/0141-5425(93)90066-8
Klaus, A. V., Kulasekera, V. L. and Schawaroch, V. (2003). Three-dimensional visualization of insect morphology using confocal laser scanning microscopy. *J. Microsc.* **212**, 107-121. doi:10.1046/j.1365-2818.2003.01235.x
Kolmann, M. A. and Huber, D. R. (2009). Scaling of feeding biomechanics in the horn shark *Heterodontus francisci*: ontogenetic constraints on durophagy. *Zoology* **112**, 351-361. doi:10.1016/j.zool.2008.11.002
Korsun, P. P., Ivanova, O. V., Afanasiev, V. L. and Kulyk, I. V. (2016). Distant Jupiter family Comet P/2011 P1 (McNaught). *Icarus* **266**, 88-95. doi:10.1016/j.icarus.2015.11.017
Lautenschlager, S. (2015). Estimating cranial musculoskeletal constraints in theropod dinosaurs. *R. Soc. Open Sci.* **2**, 150495.
Lautenschlager, S., Rayfield, E. J., Altangerel, P., Zanno, L. E. and Witmer, L. M. (2012). The endocranial anatomy of therizinosauria and its implications for sensory and cognitive function. *PLoS One* **7**, e52289. doi:10.1371/journal.pone.0052289
Lee, I. S., Kim, M. J., Yoo, D. S., Lee, Y. S., Park, S. S., Bok, G. D., Han, S. H., Chung, Y. H., Chang, B. S., Yi, Y. S. et al. (2007). Three-dimensional reconstruction of medieval child mummy in Yangju, Korea, using multi-detector computed tomography. *Ann. Anat.* **189**, 558-568. doi:10.1016/j.aanat.2007.03.005
Lockwood, C. A., Lynch, J. M. and Kimbel, W. H. (2002). Quantifying temporal bone morphology of great apes and humans: an approach using geometric morphometrics. *J. Anat.* **201**, 447-464. doi:10.1046/j.1469-7580.2002.00122.x
Lüthy, R., Bowie, J. U. and Eisenberg, D. (1992). Assessment of protein models with three-dimensional profiles. *Nature* **356**, 83-85. doi:10.1038/356083a0
Manafzadeh, A. R. and Padian, K. (2018). ROM mapping of ligamentous constraints on avian hip mobility: implications for extinct ornithodirans. *Proc. R. Soc. B* **285**, 1-9. doi:10.1098/rspb.2018.0727
Maynard Smith, J. and Savage, R. J. G. (1959). The mechanics of mammalian jaws. *Sch. Sci. Rev.* **40**, 289-301.
Middleton, K. M. and Gatesy, S. M. (2000). Theropod forelimb design and evolution. *Zool. J. Linn. Soc.* **128**, 149-187. doi:10.1111/j.1096-3642.2000.tb00160.x
Moazen, M., Curtis, N., O'Higgins, P., Evans, S. E. and Fagan, M. J. (2009). Biomechanical assessment of evolutionary changes in the lepidosaurian skull. *Proc. Natl. Acad. Sci. USA* **106**, 8273-8277. doi:10.1073/pnas.0813156106
Monteiro, L. R., Cavalcanti, M. J. and Sommer, H. J. S., III (1997). Comparative ontogenetic shape changes in the skull of Caiman species (Crocodylia, Alligatoridae). *J. Morphol.* **231**, 53-62. doi:10.1002/(SICI)1097-4687(199701)231:1<53::AID-JMOR5>3.0.CO;2-P
Mook, C. C. (1921a). Skull characters of recent Crocodilia: with notes on the affinities of the recent genera. *Bull. Am. Mus. Nat. Hist.* **44**, 123-268.
Mook, C. C. (1921b). Individual and age variation in the skulls of recent Crocodilia. *Bull. Am. Mus. Nat. Hist.* **44**, 55-66.
Norton, J. J. (1966). *Ternary Diagrams of the Quartz-feldspar Content of Pegmatites in Colorado*. US Government Printing Office.
Othmer, D. and Tobias, P. (1942). Liquid-liquid extraction data - the line correlation. *Ind. Eng. Chem.* **34**, 693-696. doi:10.1021/ie50390a600
Pfaller, J. B., Gignac, P. M. and Erickson, G. M. (2011). Ontogenetic changes in jaw-muscle architecture facilitate durophagy in the turtle *Sternotherus minor*. *J. Exp. Biol.* **214**, 1655-1667. doi:10.1242/jeb.048090
Piras, P., Buscalioni, A. D., Teresi, L., Raia, P., Sansalone, G., Kotsakis, T. and Cubo, J. (2014). Morphological integration and functional modularity in the crocodilian skull. *Integr. Zool.* **9**, 498-516. doi:10.1111/1749-4877.12062
Preusker, F., Scholten, F., Matz, K.-D., Roatsch, T., Willner, K., Hviid, S. F., Knollenberg, J., Jorda, L., Gutiérrez, P. J., Kührt, E. et al. (2015). Shape model, reference system definition, and cartographic mapping standards for comet 67P/Churyumov-Gerasimenko – Stereo-photogrammetric analysis of Rosetta/OSIRIS image data. *Astron. Astrophys. Suppl. Ser.* **583**, A33. doi:10.1051/0004-6361/201526349
Rayfield, E. J. (2007). Finite element analysis and understanding the biomechanics and evolution of living and fossil organisms. *Annu. Rev. Earth Planet. Sci.* **35**, 541-576. doi:10.1146/annurev.earth.35.031306.140104
Santana, S. E., Dumont, E. R. and Davis, J. L. (2010). Mechanics of bite force production and its relationship to diet in bats. *Funct. Ecol.* **24**, 776-784. doi:10.1111/j.1365-2435.2010.01703.x
Schachner, E. R., Hutchinson, J. R. and Farmer, C. (2013). Pulmonary anatomy in the Nile crocodile and the evolution of unidirectional airflow in Archosauria. *PeerJ* **1**, e60. doi:10.7717/peerj.60
Sellers, K. C., Middleton, K. M., Davis, J. L. and Holliday, C. M. (2017). Ontogeny of bite force in a validated biomechanical model of the American alligator. *J. Exp. Biol.* **220**, 2036-2046. doi:10.1242/jeb.156281
Sinclair, A. G. and Alexander, R. M. N. (1987). Estimates of forces exerted by the jaw muscles of some reptiles. *J. Zool.* **213**, 107-115. doi:10.1111/j.1469-7998.1987.tb03681.x
Snively, E., Cotton, J. R., Ridgely, R. and Witmer, L. M. (2013). Multibody dynamics model of head and neck function in Allosaurus (Dinosauria, Theropoda). *Palaeontol. Electronica* **16**, 1-29. doi:10.26879/338
Snively, E., Fahlke, J. M. and Welsh, R. C. (2015). Bone-breaking bite force of *Basilosaurus isis* (Mammalia, Cetacea) from the late Eocene of Egypt estimated by finite element analysis. *PLoS ONE* **10**, e0118380. doi:10.1371/journal.pone.0118380
Stephenson, R. S., Atkinson, A., Kottas, P., Perde, F., Jafarzadeh, F., Bateman, M., Iaizzo, P. A., Zhao, J., Zhang, H., Anderson, R. H. et al. (2017). High resolution 3-Dimensional imaging of the human cardiac conduction system from microanatomy to mathematical modeling. *Sci. Rep.* **7**, 7188. doi:10.1038/s41598-017-07694-8
Sustaita, D. (2008). Musculoskeletal underpinnings to differences in killing behavior between North American accipiters (Falconiformes: Accipitridae) and falcons (Falconidae). *J. Morphol.* **269**, 283-301. doi:10.1002/jmor.10577
Sustaita, D. and Hertel, F. (2010). In vivo bite and grip forces, morphology and prey-killing behavior of North American accipiters (Accipitridae) and falcons (Falconidae). *J. Exp. Biol.* **213**, 2617-2628.
Tsai, H. P. and Holliday, C. M. (2015). Articular soft tissue anatomy of the archosaur hip joint: Structural homology and functional implications. *J. Morphol.* **276**, 601-630. doi:10.1002/jmor.20360
Turner, A. H. and Nesbitt, S. J. (2013). Body size evolution during the Triassic archosauriform radiation. *Geological Soc. Lond. Special Publications* **379**, 573-597. doi:10.1144/SP379.15
Vincent, S. E., Moon, B. R., Herrel, A. and Kley, N. J. (2007). Are ontogenetic shifts in diet linked to shifts in feeding mechanics? Scaling of the feeding apparatus in the banded watersnake *Nerodia fasciata*. *J. Exp. Biol.* **210**, 2057-2069. doi:10.1242/jeb.02779
Witmer, L. M. (1995). The extant phylogenetic bracket and the importance of reconstructing soft tissue in fossils. In *Functional Morphology in Vertebrate Paleontology* (ed. Thomason, J. J.), pp. 19-33. Cambridge University Press.

Witmer, L. M. and Rose, K. D. (1991). Biomechanics of the jaw apparatus of the gigantic Eocene bird Diatryma: implications for diet and mode of life. *Paleobiology* **17**, 95-120. doi:10.1017/S0094837300010435
Witmer, L. M., Sampson, S. D. and Solounias, N. (1999). The proboscis of tapirs (Mammalia: Perissodactyla): A case study in novel narial anatomy. *J. Zool.* **249**, 249-267. doi:10.1111/j.1469-7998.1999.tb00763.x
Yanega, G. M. and Rubega, M. A. (2004). Hummingbird jaw bends to aid insect capture. *Nature* **428**, 615. doi:10.1038/428615a
Zemla, A. (2003). LGA: A method for finding 3D similarities in protein structures. *Nucleic Acids Res.* **31**, 3370-3374. doi:10.1093/nar/gkg571
Zusi, R. L. (1987). A feeding adaptation of the jaw articulation in New World jays (Corvidae). *Auk* **104**, 665-680. doi:10.1093/auk/104.4.665